

UCLA

UCLA Previously Published Works

Title

Toward more accurate surface properties of ceria using many-body perturbation theory.

Permalink

<https://escholarship.org/uc/item/4zj4j8jd>

Journal

The Journal of Chemical Physics, 159(5)

ISSN

0021-9606

Authors

Wei, Ziyang
Yan, George
Sautet, Philippe

Publication Date

2023-08-07

DOI

10.1063/5.0161084

Supplemental Material

<https://escholarship.org/uc/item/4zj4j8jd#supplemental>

Copyright Information

This work is made available under the terms of a Creative Commons Attribution-NonCommercial-NoDerivatives License, available at <https://creativecommons.org/licenses/by-nc-nd/4.0/>

Peer reviewed

Towards More Accurate Surface Properties of Ceria Using Many-Body Perturbation Theory

Ziyang Wei,^{*,†} George Yan,[‡] and Philippe Sautet^{*,†,‡}

[†]*Department of Chemistry and Biochemistry, University of California, Los Angeles, California, 90095, United States*

[‡]*Department of Chemical and Biomolecular Engineering, University of California, Los Angeles, California, 90095, United States*

E-mail: wzy@chem.ucla.edu; sautet@ucla.edu

Abstract

Despite the wide applications, the ab initio modeling of the ceria based catalyst is challenging. The partial occupation in the 4f orbitals creates a fundamental challenge for commonly used density functional theory (DFT) methods, including semilocal functionals with Hubbard U correction to force localization and hybrid functionals. In this work, we benchmark the random phase approximation (RPA) for ceria surface properties including surface energy and hydrogenation energy, compared to the results utilizing the DFT+U approach or hybrid functionals. We show that, for the latter approaches, different surface properties require opposite directions of parameter tuning. This forms a dilemma for the parameter based DFT methods, as the improvement of a certain property by tuning parameters will inevitably lead to the worsening of other properties. Our results suggest that the parameter-free many-body perturbation theory methods exemplified by RPA is a promising strategy to escape the dilemma and provide highly accurate descriptions, which will allow us to better understand the catalytic reactions in ceria related systems.

Ceria (CeO_2) has attracted growing interests¹⁻⁵ over the past decades due to its widespread applications in heterogeneous catalysis for multiple oxidation reactions⁶⁻⁸ but also for processes such as NO_x selective catalytic reduction⁹ and abatement of volatile organic compounds.¹⁰ These applications are closely related with the redox property of ceria, including at its surface. The most straightforward example is the formation of oxygen vacancies and the creation of O-X bonds (X can be hydrogen, carbon or other elements involved) at the ceria surface. In the oxygen vacancies formation processes, by switching between the oxidation states +3 and +4 for cerium, the ceria serves as an oxygen reservoir by creating and replenishing surface oxygen vacancy: when one oxygen vacancy is formed, two Ce^{4+} ions are reduced to Ce^{3+} ions. When surface hydroxyls form, a similar process happens: one Ce^{4+} ion becomes one Ce^{3+} ion. This ability of Ceria to interact with hydrogen also provides remarkable properties as hydrogenation catalysts, and ceria is a very selective catalyst for alkyne hydrogenation.¹¹ It is hence of utmost importance to reach a fundamental understanding of the redox surface chemistry of ceria. For all these elementary processes happening at the surface, the surface energy is another essential parameter as it is negatively related to the adsorption strength. Therefore, to better understand and design ceria related materials, a correct description of both the surface energy and the surface redox property is a critical first step.

Nevertheless, the description of such dihydrogen adsorption and surface hydroxyl formation poses a great challenge for computational modeling as it involves the reduction of cerium to the oxidation state +3: the cerium ions in oxidation state +4 have empty 4f orbitals and do not represent a serious problem; the difficulty sets in when the oxidation state 3+ is introduced, as the 4f orbitals becomes partially populated with electrons. Due to the self-interaction error¹² (SIE) intrinsic to density functional theory^{13,14} (DFT) exchange correlation functionals, the electrons become over-delocalized and spill over all the cerium ions. Different strategies have been proposed to overcome this shortcoming, and two most commonly used ones are (1) the DFT+U approach,¹⁵⁻¹⁷ which corrects the semilocal DFT

functionals for on-site Coulomb correlation effects by a Hubbard-type U term,¹⁸ and (2) the hybrid functionals,¹⁹ which adds a fraction of the exact exchange to mitigate the SIE.²⁰ The self-interaction correction scheme¹² is also a possible remedy for the SIE, but the applications to ceria is generally less common compared to the aforementioned approaches. Recently, applying the many-body perturbation theory (MBPT) in its random phase approximation^{21–27} (RPA) to bulk CeO₂ and Ce₂O₃, Schäfer et al.²⁸ have shown that the bulk properties, including the redox enthalpy, can be correctly described with RPA, hence providing an ab initio approach fundamentally better grounded than tuning the U parameter in the DFT+U approach or the exact exchange ratio in the hybrid functional. Application of RPA to the more catalysis-related yet more challenging CeO₂ surface properties remains unexplored.

In this work, we model critical properties of the ceria(111) surface including the surface energy and the hydrogenation energy using RPA. We show that the RPA energetics match significantly better with the experimental data, compared to the more commonly used methods such as the Perdew-Burke-Ernzerhof²⁹ (PBE) functional with a +U correction and the HSE06³⁰ hybrid functional. Our results suggest that the commonly used methods cannot describe different surface properties simultaneously, as this requires opposite directions of parameter tuning. In contrast, the MBPT method such as RPA is a promising parameter-free strategy, considering its accuracy and its well-defined theoretical framework for further improvement.

We briefly summarize the RPA energy formulas here, and more details can be found in the literature.^{21–27} The total RPA energy consists of the Hartree-Fock component (EXX) calculated for the occupied orbitals which includes the Hartree-Fock exchange, the Hartree energy, the kinetic energy, and the Ewald energy of the ions and the RPA correlation component based on both the occupied and unoccupied orbitals:

$$E^{RPA} = E^{EXX}([\psi_{occ}]) + E_c^{RPA}([\psi_{occ}, \psi_{uocc}]) \quad (1)$$

where the RPA correlation energy is calculated as:

$$E_c = \int_0^\infty \frac{d\omega}{2\pi} \text{Tr}\{\ln[1 - \chi(i\omega)\nu] + \chi(i\omega)\nu\} \quad (2)$$

where χ is the response function and ν is the the Coulomb kernel. In this work, the RPA energies are based on the HSE06 single-electron orbitals, i.e., we use RPA@HSE06. All the calculations were performed with the VASP code³¹ and further details are provided in the Supporting Information (SI). In this work, we do not consider the second order Møller–Plesset perturbation theory³² (MP2) method, since it has been discussed³³ that the MP2 method is expected to work well for weakly polarizable systems, whereas the RPA fits better for densely packed strongly polarizable solids. The polarizability of ceria is shown to be large, ca. 25 times the vacuum value.³⁴ Consistently with this, it has been shown that RPA describes the bulk properties better than MP2²⁸ and we therefore focus on RPA.

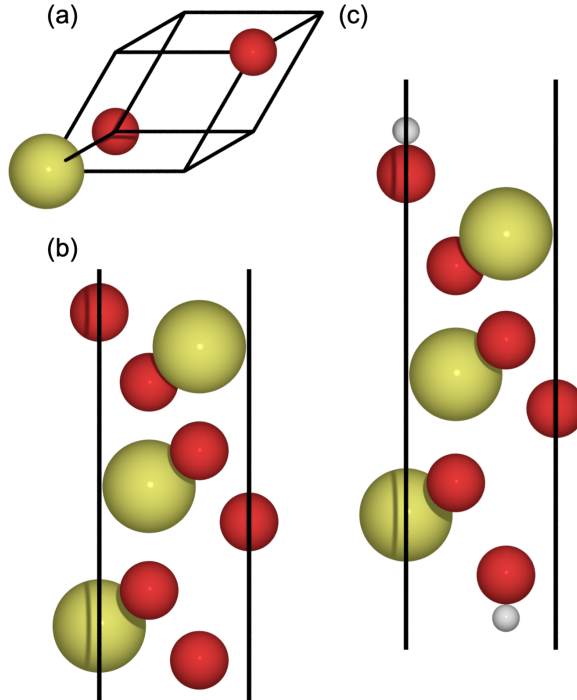


Figure 1: (a) The unit cell of the CeO₂. (b) The side view of a $p(1 \times 1)$ CeO₂(111) surface slab. (c) The side view of a symmetrically hydrogenated $p(1 \times 1)$ CeO₂(111) surface slab. Ce atoms are shown as yellow, O atoms red, and H atoms light grey.

We first investigate the surface energy of the ceria(111) facet, comparing the results of the PBE functional with a +U correction, the HSE06 functional, and the RPA method. The surface energy is calculated as

$$E_{\sigma} = \frac{E_{slab} - n * E_{bulk}}{\sigma} \quad (3)$$

where E_{slab} is the energy of a symmetric slab with two equivalent surfaces (as shown in Fig. 1b), and n is the number of formula units in this slab (3 for our model). E_{bulk} is the bulk energy per formula (CeO_2) and σ is the surface area. The bulk and surface models used are shown in Fig. 1. We performed the convergence test regarding the model thickness using the PBE+U scheme ($U=4.5$ eV), and showed that increasing the model thickness from 3 to 6 trilayers decreases the surface energy by 0.02 J/m^2 (see SI for the details). The RPA result, 1.09 J/m^2 , matches well with the experimental value,³⁵ $1.23 \pm 0.22 \text{ J/m}^2$. However, the PBE+U ($U=4.5$ eV) value, 0.70 J/m^2 and the HSE06 value, 0.76 J/m^2 , are underestimated by at least 0.31 and 0.25 J/m^2 , respectively. We note that our calculated PBE+U ($U=4.5$ eV) and HSE06 values show good consistency with literature values.⁴

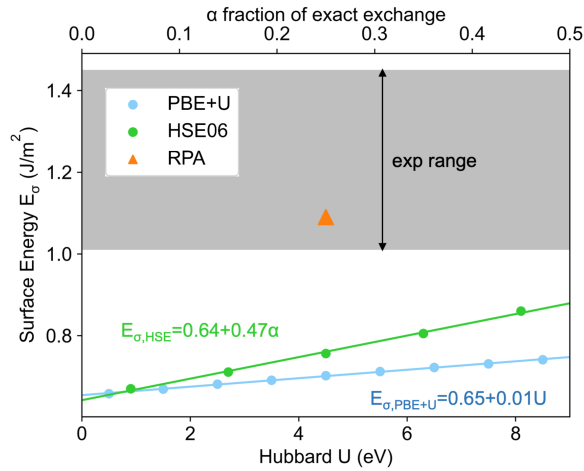


Figure 2: $\text{CeO}_2(111)$ surface energy calculated at different levels of theory and with varying parameters. The Hubbard parameter U for the PBE+U scheme is represented by the lower axis, and the fraction of Fock exchange α for the HSE06 functional by the upper axis. The shaded region indicates the experimental range.³⁵ The RPA results does not depend on any parameter, and is arbitrarily placed in the middle of the horizontal axis.

Seemingly it is a handy solution to obtain better agreement with the experimental surface energy by tuning the parameters in the DFT methods, i.e., the U value in the DFT+ U approach and the exact exchange ratio in the hybrid functional. We therefore conducted calculations with varying U values ($U=0.5-8.5$ eV) and exact exchange ratios ($\alpha=0.05-0.45$). The results are shown in Fig. 2. The energetics of both methods show a linear relationship between the surface energy and the tunable parameter. The linearity is similar to the bulk case discussed by Schäfer et al.,²⁸ where the authors focus on the reaction enthalpy between bulk Ce_2O_3 and CeO_2 phases. The details of the linear trends of the surface energy are however different from the bulk property case. For the surface energy case, the slope is positive, being consistent with literatures,³⁶ and the slope magnitude is small. For the bulk case, the slope is negative and the slope magnitude is large. Such differences are expected: for the $\text{CeO}_2(111)$ surface energy, both the CeO_2 bulk part and the $\text{CeO}_2(111)$ surface of the slab contain only (formally) Ce^{4+} ions and the influence of the parameters is significantly smaller compared to the case where Ce^{3+} is involved. Consequently, this leads to the small magnitude of the slope, which is unable to match the experimental value in a reasonable interval. To obtain agreement with the lower bound of the experimental surface energy, a U value of ca. 35 eV is needed, which is far outside of the typical range of U values.²⁸ The case for the exact exchange ratio in the HSE06 functional is slightly better: ca. 0.76 is needed to match with the lower bound of the experimental value. However, the 0.76 ratio deviates heavily from the 0.25 ratio derived from the adiabatic connection formula, and is also unsuitable considering the electronic structure. As shown by Schäfer et al.,²⁸ the band gap of bulk Ce_2O_3 is predicted to be ca. 6 eV with this ratio, which is heavily overestimated compared to the experimental value, 2.4 eV.³⁷ Therefore, both DFT methods cannot provide a reasonable description of the surface energy for $\text{CeO}_2(111)$ within a physically meaningful range of the parameters.

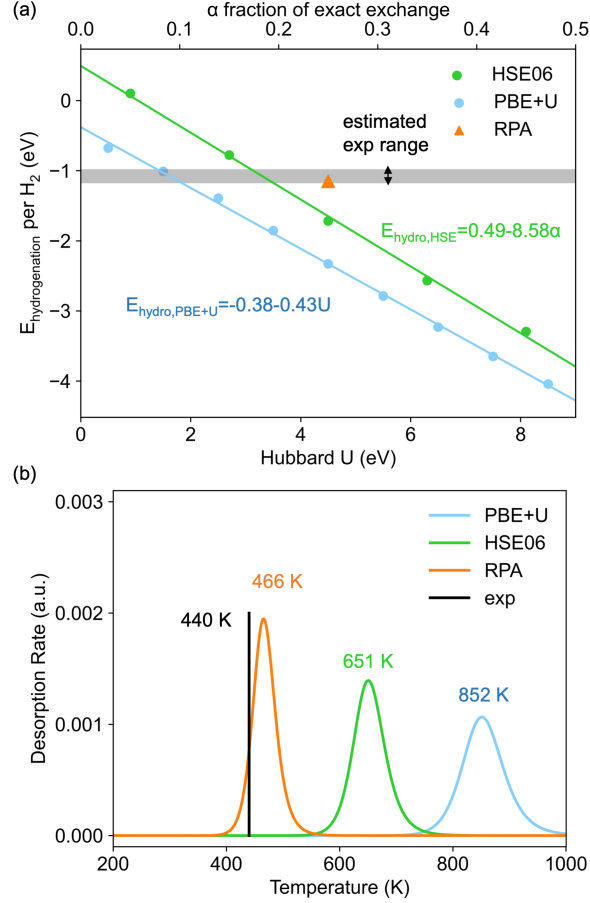


Figure 3: (a) The hydrogenation energy on the $\text{CeO}_2(111)$ facet calculated at different levels of theory and with varying parameters. The Hubbard parameter U for the PBE+U scheme is represented by the lower axis, and the fraction of Fock exchange α for the HSE06 functional by the upper axis. The experimental value, -1.08 eV, is evaluated by interpolating several data points with simulated desorption peak position around 440 K (details can be found in the SI). The error bar is estimated to be 0.1 eV. (b) The simulated temperature-programmed desorption results using the energetics of RPA, PBE+U ($U=4.5$ eV), and HSE06 ($\alpha=0.25$). The experimental peak locates at ca. 440 K.³⁸

We then investigate the hydrogenation energy, which is defined as

$$E_{\text{hydrogenation}} = E_{*H} - E_* - E_{\text{H}_2,\text{ref}} \quad (4)$$

where E_{*H} is the energy of the hydrogenated surface at full coverage, E_* is the energy of the bare surface, and $E_{\text{H}_2,\text{ref}}$ is the gas phase hydrogen molecule energy. We note that we use a symmetric hydrogenated surface (as shown in Fig. 1c) and our hydrogenation

energy is normalized to per H₂ molecule. The results are shown in Fig. 3a. One difficulty here is that the experimental value of hydrogenation energy on the ceria(111) facet is not directly available. Therefore, we compare simulated temperature-programmed desorption (TPD) results (details can be found in the SI) with experimental results. We estimated the potential energy barrier in the adsorption direction to be ca. 0.4 eV. This value is derived from the fact that Werner et al.³⁹ observed D₂ dissociation on CeO₂(111) at 300 K and 10 mbar. As the time scale for a spectroscopic measurement should be in the order of minutes or faster, only chemical processes with a characteristic time scale of 10² seconds or below could be observed by spectroscopic techniques. Which, within transition state theory, returns a range of 0.8-1.0 eV as the upper bound of the free energy barrier. Subtracting away the translational, rotational, and pressure contributions to the total free energy of the D₂ gas reactant (-0.48 eV at 300 K and 10 mbar using standard statistical mechanical equations), we take here an estimate of 0.4 eV as the potential energy barrier for the dissociation of D₂. It is worth mentioning that this effective activation barrier estimated from experiment is much lower than the barrier calculated on perfect CeO₂(111) terrace models at the GGA+U³⁹ and hybrid functional^{40,41} levels, ca. 1 eV. Nevertheless, it is important to note that the CeO₂(111) thin films can expose defects such as step edges, where dissociation could be easier. Chen et al.³⁸ had grown their film on Cu(111), while Werner et al.³⁹ had grown theirs on Ru(0001). Step edges are clearly visible from STM images^{42,43} of CeO₂(111) films grown on such substrates.

The simulated TPD results using energetics at different levels are shown in Fig. 3b. The RPA value, -1.15 eV, corresponding to a peak at 466 K, gives a good agreement with the experimental desorption peak around 440 K.³⁸ We note that the match should not be overemphasized considering the large error bar, ca. 0.3 eV, from both the experimental and computational sides: the experimental peak is weak and broad and the computational value for the desorption temperature relies on an estimated energy barrier. Nevertheless, the PBE+U (U=4.5 eV) value, -2.33 eV, and the HSE06 ($\alpha=0.25$) value, -1.72 eV, both

correspond to a peak located at a heavily overestimated temperature, 651 K and 852 K, respectively. The predicted desorption temperature will be further overestimated if the calculated terrace desorption barrier value, 1 eV, is used. To make the comparison between energies more straightforward, we evaluate the experimental hydrogenation energy to be ca. -1.08 eV by interpolating several data points with simulated desorption peak position around 440 K (details can be found in the SI). From the energetic perspective, the RPA value is inline with the experimental value while PBE+U (U=4.5 eV) and HSE06 ($\alpha=0.25$) overbinds the hydrogen by 1.25 eV and 0.64 eV, respectively.

There are two other factors worth considering when interpreting the calculations. The first one is the coverage effect, as the experimental results may correspond to a lower coverage. We performed calculations with the PBE+U method (U=4.5 eV) and found that compared to the full coverage cases presented in this work, one fourth coverage gives a hydrogenation energy lowered by 0.13 eV per H₂. The second factor is the strain effect: after reduction, the Ce³⁺ ions are with larger radius compared to the Ce⁴⁺ ions. PBE+U (U=4.5 eV) results show that if a fully hydrogenated surface is allowed to relax, the hydrogenation energy per H₂ will become 0.09 eV more negative. However, considering the experimental coverage is probably lower than 1, the contribution from the strain effect will be just a portion of -0.09 eV. Since the experimental coverage is not reported, we leave an estimate for these contributions as up to -0.2 eV but do not directly sum these into the energies presented.

For the DFT results, it is possible to obtain a better match with the experimental hydrogenation energy by tuning the Hubbard U parameter or the exact exchange ratio. The linear relationships between the hydrogenation energy and the tunable parameters are shown in Fig. 3a. Different from the surface energy case, the slope in the hydrogenation energy case is negative, similar to the bulk reaction enthalpy case discussed by Schäfer et al.²⁸ This can be explained as both the hydrogenation energy in this work and the bulk reaction enthalpy used by Schäfer et al.²⁸ are linked with the energy variation when replacing Ce⁴⁺ by Ce³⁺. Consequently, to obtain a better match with experimental hydrogenation energy, a weaker

localization is needed: tuning the U to ca. 1.63 eV or the exact exchange ratio to 0.18 provides a match with the experimental value. If we only consider the hydrogenation energy, parameter tuning is indeed acceptable to obtain a reasonable agreement with experimental data.

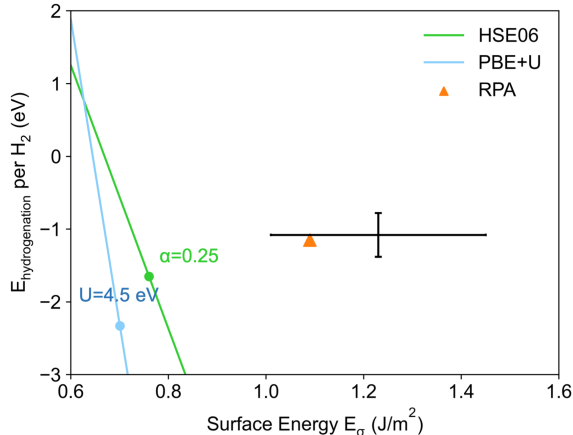


Figure 4: $\text{CeO}_2(111)$ surface energy and hydrogenation energy relationship calculated with methods at different levels. The results of PBE+U ($U=4.5$ eV) and HSE06 ($\alpha=0.25$) are shown as filled circles, while the lines show the change upon modifying the parameters. Experimental values are shown with error bar.^{35,38}

However, combining the two aforementioned aspects, our results clearly show the awkward situation faced by the commonly used DFT methods for the ceria surface system, as shown in Fig. 4. With the most widely used parameters ($U=4.5$ eV and $\alpha=0.25$), neither the surface energy nor the hydrogenation energy can be described with a reasonable accuracy. In principle, the parameters in the DFT methods can be tuned to match with experimental results. Nevertheless, as we discussed, three fundamental problems are encountered: (1) for certain property, such as the surface energy, reasonable agreement can only be reached by tuning the parameters to an extremely unphysical value (Hubbard $U=35$ eV). (2) changing the parameters from standard values will also negatively affect other electronic properties (for example, the band gap). (3) more importantly, different surface properties requires opposite directions of tuning. Accurate surface energy requires a stronger localization whilst accurate hydrogenation energy requires a weaker localization. This forms a dilemma similar

to the one being encountered in the CO puzzle.⁴⁴ With the commonly used DFT methods, a reasonable description of multiple surface properties can never be obtained simultaneously: one can only get a better description of the surface redox property by sacrificing the surface energy, or vice versa. However, both properties are involved in surface catalytic processes and thence essential for an accurate description of catalytic mechanisms in ceria based systems. Our results emphasize that MBPT methods exemplified by RPA are a promising solution for these systems.

Several extensions can be explored in the future. The first aspect concerns the oxygen vacancy formation, which is essential to a large number of catalytic processes in the ceria system. Paier et al.^{4,45} have mentioned that compared to the experimental estimation^{2,46} of 4.2 ± 0.3 eV, PBE+U (U=4-6 eV) underestimates the defect formation energy by 1.5 eV and HSE underestimates it by 0.5-0.8 eV. Modeling of the oxygen vacancy, however, requires at least a $p(2 \times 2)$ ceria(111) surface model. This imposes extremely heavy requirements on memory at the RPA level and our attempts failed. We note that the recent cubic scaling RPA implementation⁴⁷ does not solve this problem. Instead, it requires more memory compared to the earlier quaternary implementation. The second aspect is to go beyond RPA: various methods⁴⁸⁻⁵³ to improve further based on RPA have been discussed in recent years, including a local correction to the coupled cluster (CC) level,⁵³ showing a clear way towards chemical accuracy with the MBPT methods. One simplest and probably most affordable step forward is to include the second order screened exchange⁴⁸⁻⁵⁰ (SOSEX) terms. However, for periodic codes such as VASP and FHI-aims, to the best of the authors' knowledge, the SOSEX code is not publicly available. Moreover, we note that the calculations of the surface systems with RPA is already at the cutting edge of current computational power. It is therefore questionable whether the RPA+SOSEX approach (with a N^5 scaling where N is the system size, compared to N^4 or N^3 scaling of RPA) is affordable for such systems. Note that even for the smaller bulk ceria system, calculations are still limited to RPA with renormalized second order exchange²⁸ (rSOX), which is an approximated version of RPA+SOSEX. That being

said, once the computational cost becomes affordable, a systematic way towards even better accuracy has been established for the MBPT methods: RPA to RPA+SOSEX and eventually RPA+SOSEX+local CC corrections. Considering the large error bar in the experimental measurements (0.22 eV for surface energy,³⁵ 0.3 eV for oxygen vacancy formation energy,⁴⁵ and no direct experimental measurement of the hydrogenation energy), the MBPT results may serve as computational benchmark and aid the development of novel functionals or machine learning methods.

In conclusion, we present a benchmark of MBPT methods on the surface properties of ceria, compared to the results utilizing common parameter based DFT methods. We show that the RPA method overcomes essential limits of the DFT+U scheme and of hybrid functionals. (1) The accurate description of surface energy and hydrogenation energy can be obtained using RPA, while the parameter based methods require tuning the parameters to unphysical values. (2) More importantly, with the DFT+U scheme or the HSE06 hybrid functional, the surface energy can only be improved by sacrificing the surface redox description, and vice versa. Consequently, it is impossible to simultaneously describe different surface properties with a reasonable accuracy. In contrast to the parameter based DFT methods, MBPT methods exemplified by RPA show an unprecedented agreement with the experimental results and also a systematic approach towards further improvement, which will allow us to better understand the catalytic reactions in ceria related systems. We also expect that the MBPT results may serve as computational benchmark to facilitate the development of novel efficient functionals or machine learning methods for fast calculations.

Supplementary Material

computational details; k-point mesh and model thickness convergence tests; raw RPA energetics; desorption simulation details

Acknowledgement

The calculations were performed on the Hoffman2 cluster at UCLA Institute for Digital Research and Education (IDRE) and the Extreme Science and Engineering Discovery Environment (XSEDE),⁵⁴ which is supported by National Science Foundation grant number ACI-1548562, through allocation TG-CHE170060. The authors thank Tobias Schäfer for helpful discussions about norm-conserving PAW potentials.

References

- (1) Trovarelli, A.; De Leitenburg, C.; Boaro, M.; Dolcetti, G. The utilization of ceria in industrial catalysis. *Catalysis today* **1999**, *50*, 353–367.
- (2) Gorte, R. J. Ceria in catalysis: From automotive applications to the water–gas shift reaction. *AIChE journal* **2010**, *56*, 1126–1135.
- (3) Trovarelli, A. *Catalysis by ceria and related materials*; World Scientific, 2002; Vol. 2.
- (4) Paier, J.; Penschke, C.; Sauer, J. Oxygen defects and surface chemistry of ceria: quantum chemical studies compared to experiment. *Chemical reviews* **2013**, *113*, 3949–3985.
- (5) Fadzil, N. A. M.; Rahim, M. H. A.; Maniam, G. P. Brief review of ceria and modified ceria: synthesis and application. *Materials Research Express* **2018**, *5*, 085019.
- (6) Centeno, M. A.; Ramírez Reina, T.; Ivanova, S.; Laguna, O. H.; Odriozola, J. A. Au/CeO₂ catalysts: structure and CO oxidation activity. *Catalysts* **2016**, *6*, 158.
- (7) Rodriguez, J. A.; Grinter, D. C.; Liu, Z.; Palomino, R. M.; Senanayake, S. D. Ceria-based model catalysts: fundamental studies on the importance of the metal–ceria interface in CO oxidation, the water–gas shift, CO₂ hydrogenation, and methane and alcohol reforming. *Chemical Society Reviews* **2017**, *46*, 1824–1841.

- (8) Datta, S.; Torrente-Murciano, L. Nanostructured faceted ceria as oxidation catalyst. *Current opinion in chemical engineering* **2018**, *20*, 99–106.
- (9) Gu, Y.; Epling, W. S. Passive NO_x adsorber: An overview of catalyst performance and reaction chemistry. *Applied Catalysis A: General* **2019**, *570*, 1–14.
- (10) Sun, C.; Li, H.; Chen, L. Nanostructured ceria-based materials: synthesis, properties, and applications. *Energy & Environmental Science* **2012**, *5*, 8475–8505.
- (11) Vilé, G.; Bridier, B.; Wichert, J.; Pérez-Ramírez, J. Ceria in hydrogenation catalysis: high selectivity in the conversion of alkynes to olefins. *Angewandte Chemie* **2012**, *124*, 8748–8751.
- (12) Perdew, J. P.; Zunger, A. Self-interaction correction to density-functional approximations for many-electron systems. *Physical Review B* **1981**, *23*, 5048.
- (13) Hohenberg, P.; Kohn, W. Inhomogeneous Electron Gas. *Phys. Rev.* **1964**, *136*, B864–B871.
- (14) Kohn, W.; Sham, L. Self-Consistent Equations Including Exchange and Correlation Effects. *Phys. Rev.* **1965**, *140*, A1133–A1138.
- (15) Chanier, T.; Sargolzaei, M.; Opahle, I.; Hayn, R.; Koepf, K. LSDA+ U versus LSDA: Towards a better description of the magnetic nearest-neighbor exchange coupling in Co- and Mn-doped ZnO. *Physical Review B* **2006**, *73*, 134418.
- (16) Himmetoglu, B.; Floris, A.; De Gironcoli, S.; Cococcioni, M. Hubbard-corrected DFT energy functionals: The LDA+ U description of correlated systems. *International Journal of Quantum Chemistry* **2014**, *114*, 14–49.
- (17) Pemmaraju, C. D.; Archer, T.; Sánchez-Portal, D.; Sanvito, S. Atomic-orbital-based approximate self-interaction correction scheme for molecules and solids. *Physical Review B* **2007**, *75*, 045101.

- (18) Dudarev, S. L.; Botton, G. A.; Savrasov, S. Y.; Humphreys, C.; Sutton, A. P. Electron-energy-loss spectra and the structural stability of nickel oxide: An LSDA+ U study. *Physical Review B* **1998**, *57*, 1505.
- (19) Da Silva, J. L.; Ganduglia-Pirovano, M. V.; Sauer, J.; Bayer, V.; Kresse, G. Hybrid functionals applied to rare-earth oxides: The example of ceria. *Physical Review B* **2007**, *75*, 045121.
- (20) Becke, A. D. A new mixing of Hartree–Fock and local density-functional theories. *The Journal of chemical physics* **1993**, *98*, 1372–1377.
- (21) Langreth, D.; Perdew, J. The exchange-correlation energy of a metallic surface. *Solid State Commun.* **1975**, *17*, 1425–1429.
- (22) Gunnarsson, O.; Lundqvist, B. Exchange and correlation in atoms, molecules, and solids by the spin-density-functional formalism. *Phys. Rev. B* **1976**, *13*, 4274–4298.
- (23) Langreth, D. C.; Perdew, J. P. Exchange-correlation energy of a metallic surface: Wave-vector analysis. *Phys. Rev. B* **1977**, *15*, 2884–2901.
- (24) Niquet, Y.; Fuchs, M.; Gonze, X. Exchange-correlation potentials in the adiabatic connection fluctuation-dissipation framework. *Phys. Rev. A* **2003**, *68*, 032507.
- (25) Dahlen, N. E.; van Leeuwen, R.; von Barth, U. Variational energy functionals of the Green function and of the density tested on molecules. *Phys. Rev. A* **2006**, *73*, 012511.
- (26) Harl, J.; Schimka, L.; Kresse, G. Assessing the quality of the random phase approximation for lattice constants and atomization energies of solids. *Phys. Rev. B* **2010**, *81*, 115126.
- (27) Yang, W.; Mori-Sánchez, P.; Cohen, A. J. Extension of many-body theory and approximate density functionals to fractional charges and fractional spins. *J. Chem. Phys.* **2013**, *139*, 104114.

- (28) Schäfer, T.; Daelman, N.; Lopez, N. Cerium oxides without U: The role of many-electron correlation. *The Journal of Physical Chemistry Letters* **2021**, *12*, 6277–6283.
- (29) Perdew, J. P.; Burke, K.; Ernzerhof, M. Generalized Gradient Approximation Made Simple. *Phys. Rev. Lett.* **1996**, *77*, 3865–3868.
- (30) Krukau, A. V.; Vydrov, O. A.; Izmaylov, A. F.; Scuseria, G. E. Influence of the exchange screening parameter on the performance of screened hybrid functionals. *J. Chem. Phys.* **2006**, *125*, 224106.
- (31) Kresse, G.; Hafner, J. Ab initio molecular dynamics for liquid metals. *Phys. Rev. B* **1993**, *47*, 558.
- (32) Møller, C.; Plesset, M. S. Note on an approximation treatment for many-electron systems. *Physical review* **1934**, *46*, 618.
- (33) Grüneis, A.; Marsman, M.; Kresse, G. Second-order Møller–Plesset perturbation theory applied to extended systems. II. Structural and energetic properties. *The Journal of Chemical Physics* **2010**, *133*, 074107.
- (34) Gürel, T.; Eryiğit, R. Ab initio pressure-dependent vibrational and dielectric properties of CeO₂. *Physical Review B* **2006**, *74*, 014302.
- (35) Hayun, S.; Ushakov, S. V.; Navrotsky, A. Direct measurement of surface energy of CeO₂ by differential scanning calorimetry. *Journal of the American Ceramic Society* **2011**, *94*, 3679–3682.
- (36) Zhao, Q.; Kulik, H. J. Stable surfaces that bind too tightly: Can range-separated hybrids or DFT+ U improve paradoxical descriptions of surface chemistry? *The journal of physical chemistry letters* **2019**, *10*, 5090–5098.
- (37) Herper, H. C.; Vekilova, O. Y.; Simak, S. I.; Di Marco, I.; Eriksson, O. Localized versus

- itinerant character of 4f-states in cerium oxides. *Journal of Physics: Condensed Matter* **2020**, *32*, 215502.
- (38) Chen, B.; Ma, Y.; Ding, L.; Xu, L.; Wu, Z.; Yuan, Q.; Huang, W. Reactivity of hydroxyls and water on a CeO₂ (111) thin film surface: the role of oxygen vacancy. *The Journal of Physical Chemistry C* **2013**, *117*, 5800–5810.
- (39) Werner, K.; Weng, X.; Calaza, F.; Sterrer, M.; Kropp, T.; Paier, J.; Sauer, J.; Wilde, M.; Fukutani, K.; Shaikhutdinov, S., et al. Toward an understanding of selective alkyne hydrogenation on ceria: on the impact of O vacancies on H₂ interaction with CeO₂ (111). *Journal of the American Chemical Society* **2017**, *139*, 17608–17616.
- (40) García-Melchor, M.; López, N. Homolytic products from heterolytic paths in H₂ dissociation on metal oxides: the example of CeO₂. *The Journal of Physical Chemistry C* **2014**, *118*, 10921–10926.
- (41) Brugnoli, L.; Pedone, A.; Menziani, M. C.; Adamo, C.; Labat, F. H₂ dissociation and water evolution on silver-decorated CeO₂ (111): a hybrid density functional theory investigation. *The Journal of Physical Chemistry C* **2019**, *123*, 25668–25679.
- (42) Dvorak, F.; Stetsovych, O.; Steger, M.; Cherradi, E.; Matolínová, I.; Tsud, N.; Skoda, M.; Skála, T.; Myslivecek, J.; Matolín, V. Adjusting morphology and surface reduction of CeO₂ (111) thin films on Cu (111). *The Journal of Physical Chemistry C* **2011**, *115*, 7496–7503.
- (43) Nilius, N.; Kozlov, S. M.; Jerratsch, J.-F.; Baron, M.; Shao, X.; Vines, F.; Shaikhutdinov, S.; Neyman, K. M.; Freund, H.-J. Formation of one-dimensional electronic states along the step edges of CeO₂ (111). *ACS nano* **2012**, *6*, 1126–1133.
- (44) Schimka, L.; Harl, J.; Stroppa, A.; Grüneis, A.; Marsman, M.; Mittendorfer, F.; Kresse, G. Accurate surface and adsorption energies from many-body perturbation theory. *Nat. Mater.* **2010**, *9*, 741–744.

- (45) Paier, J. Hybrid density functionals applied to complex solid catalysts: Successes, limitations, and prospects. *Catalysis Letters* **2016**, *146*, 861–885.
- (46) Panhans, M. A.; Blumenthal, R. A thermodynamic and electrical conductivity study of nonstoichiometric cerium dioxide. *Solid State Ionics* **1993**, *60*, 279–298.
- (47) Kaltak, M.; Klimeš, J.; Kresse, G. Cubic scaling algorithm for the random phase approximation: Self-interstitials and vacancies in Si. *Physical Review B* **2014**, *90*, 054115.
- (48) Grüneis, A.; Marsman, M.; Harl, J.; Schimka, L.; Kresse, G. Making the random phase approximation to electronic correlation accurate. *J. Chem. Phys.* **2009**, *131*, 154115.
- (49) Paier, J.; Janesko, B. G.; Henderson, T. M.; Scuseria, G. E.; Grüneis, A.; Kresse, G. Hybrid functionals including random phase approximation correlation and second-order screened exchange. *The Journal of chemical physics* **2010**, *132*, 094103.
- (50) Paier, J.; Ren, X.; Rinke, P.; Scuseria, G. E.; Grüneis, A.; Kresse, G.; Scheffler, M. Assessment of correlation energies based on the random-phase approximation. *New Journal of Physics* **2012**, *14*, 043002.
- (51) Chen, G. P.; Agee, M. M.; Furche, F. Performance and scope of perturbative corrections to random-phase approximation energies. *Journal of chemical theory and computation* **2018**, *14*, 5701–5714.
- (52) Yu, J. M.; Nguyen, B. D.; Tsai, J.; Hernandez, D. J.; Furche, F. Selfconsistent random phase approximation methods. *The Journal of Chemical Physics* **2021**, *155*, 040902.
- (53) Schäfer, T.; Libisch, F.; Kresse, G.; Grüneis, A. Local embedding of coupled cluster theory into the random phase approximation using plane waves. *The Journal of Chemical Physics* **2021**, *154*, 011101.
- (54) Towns, J.; Cockerill, T.; Dahan, M.; Foster, I.; Gaither, K.; Grimshaw, A.; Hazelwood, V.; Lathrop, S.; Lifka, D.; Peterson, G. D.; Roskies, R.; Scott, J. R.; Wilkins-

Diehr, N. XSEDE: Accelerating Scientific Discovery. *Comput. Sci. Eng.* **2014**, *16*, 62–74.